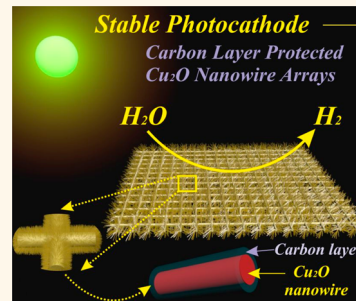


# Carbon-Layer-Protected Cuprous Oxide Nanowire Arrays for Efficient Water Reduction

Zhonghai Zhang,<sup>†,§</sup> Rubal Dua,<sup>†,§</sup> Lianbin Zhang,<sup>†</sup> Haibo Zhu,<sup>‡</sup> Hongnan Zhang,<sup>†</sup> and Peng Wang<sup>†,\*</sup>

<sup>†</sup>Water Desalination and Reuse Center, Biological and Environmental Science and Engineering Division and <sup>‡</sup>KAUST Catalysis Center, Physical Sciences and Engineering Division, King Abdullah University of Science and Technology, Thuwal 23955-6900, Saudi Arabia. <sup>§</sup>These authors contributed equally to this work.

**ABSTRACT** In this work, we propose a solution-based carbon precursor coating and subsequent carbonization strategy to form a thin protective carbon layer on unstable semiconductor nanostructures as a solution to the commonly occurring photocorrosion problem of many semiconductors. A proof-of-concept is provided by using glucose as the carbon precursor to form a protective carbon coating onto cuprous oxide ( $\text{Cu}_2\text{O}$ ) nanowire arrays which were synthesized from copper mesh. The carbon-layer-protected  $\text{Cu}_2\text{O}$  nanowire arrays exhibited remarkably improved photostability as well as considerably enhanced photocurrent density. The  $\text{Cu}_2\text{O}$  nanowire arrays coated with a carbon layer of 20 nm thickness were found to give an optimal water splitting performance, producing a photocurrent density of  $-3.95 \text{ mA cm}^{-2}$  and an optimal photocathode efficiency of 0.56% under illumination of AM 1.5G ( $100 \text{ mW cm}^{-2}$ ). This is the highest value ever reported for a  $\text{Cu}_2\text{O}$ -based electrode coated with a metal/co-catalyst-free protective layer. The photostability, measured as the percentage of the photocurrent density at the end of 20 min measurement period relative to that at the beginning of the measurement, improved from 12.6% on the bare, nonprotected  $\text{Cu}_2\text{O}$  nanowire arrays to 80.7% on the continuous carbon coating protected ones, more than a 6-fold increase. We believe that the facile strategy presented in this work is a general approach that can address the stability issue of many nonstable photoelectrodes and thus has the potential to make a meaningful contribution in the general field of energy conversion.



**KEYWORDS:** cuprous oxide · nanowire · photocathode · photocorrosion · carbon layer · water splitting

Since the pioneering work by Honda and Fujishima,<sup>1</sup> enormous efforts have been focused on exploring suitable semiconductor materials as efficient photoelectrodes in the photoelectrochemical (PEC) water splitting system for hydrogen generation. Within a PEC water splitting cell, the equilibration of the semiconductor's Fermi level with the redox potential of the electrolyte solution results in a band bending and thus generation of an electrical field, which drives the photogenerated minority charges from the semiconductor (*i.e.*, electrons for a p-type semiconductor and holes for an n-type semiconductor) toward the semiconductor/water interface, where water is either oxidized to oxygen with an n-type semiconductor (photoanode) or reduced to hydrogen with a p-type semiconductor (photocathode).<sup>2–6</sup> In terms of hydrogen generation, p-type semiconductors are advantageous over n-type ones. The electrons can be directly injected into the electrolyte on the p-type semiconductors and thus directly reduce water to

hydrogen at the p-type semiconductor/water interface while, with n-type semiconductors, the photogenerated electrons have to migrate through an external circuit before being utilized for water reduction on the counter electrode, which involves a potential energy loss.<sup>7–10</sup>

Unfortunately, of the current known natural crystal structures of semiconductors, p-type ones are much less than n-type (*e.g.*,  $\text{TiO}_2$ ,  $\text{ZnO}$ ,  $\text{Fe}_2\text{O}_3$ ,  $\text{WO}_3$ ).<sup>11–16</sup> As one of the few metal oxides that naturally show p-type conductivity,<sup>17</sup> cuprous oxide ( $\text{Cu}_2\text{O}$ ) is thought of by many as the most promising candidate for efficient photocathode material for the following reasons: (1) it has a band gap of  $\sim 2.0 \text{ eV}$ , which guarantees efficient visible light absorption;<sup>18,19</sup> (2) its conduction band lies  $0.7 \text{ eV}$  negative of the hydrogen evolution potential, which allows  $\text{Cu}_2\text{O}$  to drive off water reduction reaction as photocathode;<sup>20,21</sup> (3) the natural abundance of copper on the earth's crust makes the large-scale fabrication of a  $\text{Cu}_2\text{O}$  photoelectrode

\* Address correspondence to peng.wang@kaust.edu.sa.

Received for review December 11, 2012 and accepted January 30, 2013.

Published online January 30, 2013  
10.1021/nn3057092

© 2013 American Chemical Society

potentially competitive. However, the practical application of Cu<sub>2</sub>O in the PEC process is still limited by two main drawbacks: (1) its mismatch of the intrinsic carrier diffusion length (usually 20–100 nm)<sup>22,23</sup> with the light absorption depth near the band gap (approximately 10 μm);<sup>24</sup> and (2) its poor stability due to self-photo-corrosion in electrolyte solution.<sup>25</sup>

One-dimensional (1-D) nanostructures (e.g., nanowire, nanorod, nanotube) are known to have the capability of independently modulating a semiconductor's actual carrier diffusion length and light absorption depth and have been emerging as a promising solution to the problem of the mismatch between short carrier diffusion length and long light absorption depth, which commonly occurs with many semiconductors.<sup>12,26–29</sup> The synthesis of 1-D Cu<sub>2</sub>O was not reported until recently when Li's group<sup>30</sup> synthesized Cu<sub>2</sub>O nanowires with a chemical oxidation method and when Reisner's group reported fabrication of Cu<sub>2</sub>O nanowires *via* electrochemical anodization.<sup>31</sup> On the other hand, it has been identified that the Cu<sub>2</sub>O photocorrosion occurs at the Cu<sub>2</sub>O/electrolyte interface, so protective layer coating naturally comes as a rational strategy to keep the semiconductor from directly contacting the electrolyte solution.<sup>21,31,32</sup> For this strategy to be successful, the protective layer must meet the following criteria: (1) it must be dense enough so that it can block the aqueous electrolyte solution from accessing the semiconductor surface; (2) it must be thin enough so that it does not negatively interfere with the light absorption of the semiconductor; (3) it must be conductive so that it can transmit minority carriers from the semiconductor into the electrolyte solution.

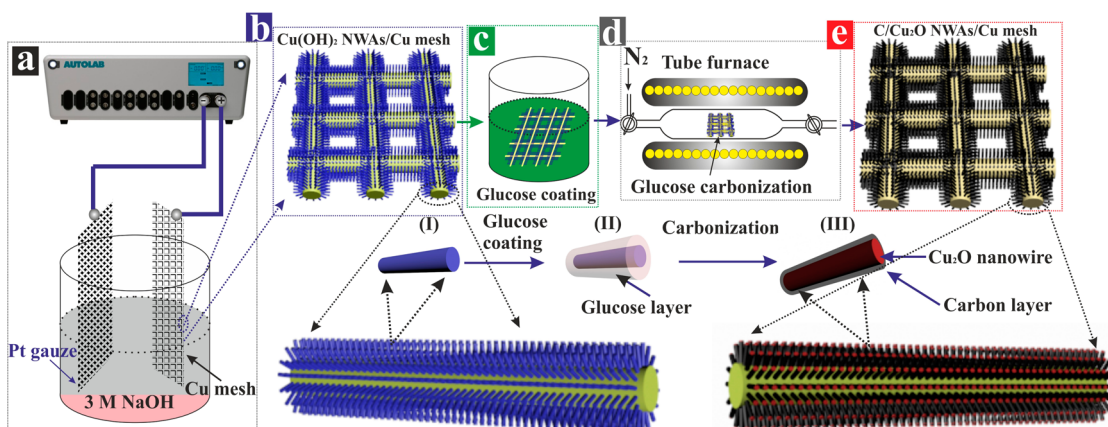
Although significant research efforts have been invested in coming up with a scalable, facile, cheap, and environmentally friendly method to synthesize a coating-layer-protected and thus highly stable Cu<sub>2</sub>O-based photocathode, they are met only with limited success. Recently, Paracchino *et al.* made a considerable stride in increasing Cu<sub>2</sub>O photocathode's resistance to photocorrosion through atomic layer deposition of multiple protective layers, but the inherent complexity of the fabrication process significantly limits its possibility of scaling up.<sup>21,32</sup> Our group also reported an *in situ* Cu<sub>2</sub>O protection strategy with CuO film as a protective layer, but it is not suitable for 1-D nanostructures.<sup>33</sup> Also a spin-coating-based procedure for coating a layer of metal oxide cocatalyst (NiO-Ni(OH)<sub>2</sub>) on presynthesized Cu<sub>2</sub>O was suggested recently for improving the photostability of the Cu<sub>2</sub>O photocathode.<sup>31</sup>

Carbon material is known to have superior conductivity, nontoxicity, and high strength, and the feasibility of solution-based carbon precursor inspires the idea of forming a thin carbon coating layer on 1-D nanostructures to protect an otherwise nonstable semiconductor-based photoelectrode.<sup>34,35</sup> In this study, we propose and demonstrate a solution-based carbon precursor

coating (*i.e.*, glucose solution) combined with subsequent carbonization to be an effective strategy to form a thin protective carbon layer on radial Cu<sub>2</sub>O nanowire arrays (NWAs). The Cu<sub>2</sub>O NWAs were grown *in situ* during the carbonization/annealing step from Cu(OH)<sub>2</sub> NWAs, which were synthesized directly on a Cu mesh using an electrochemical anodization method. The thus-synthesized material serves as an efficient and extraordinarily stable photocathode for PEC water splitting. Also, since the protective layer is a metal/co-catalyst-free pure carbon layer, coated using a simple solution-based approach instead of costly vapor deposition, it makes the overall synthesis highly cost-effective and easily scalable. We believe the proposed approach has the potential to address the stability issue of many nonstable photoelectrodes and thus can make a significant contribution in the field of energy conversion.

## RESULTS AND DISCUSSION

Scheme 1 presents the design and synthesis strategy of the carbon-layer-protected Cu<sub>2</sub>O NWAs on Cu mesh (C/Cu<sub>2</sub>O NWAs/Cu mesh) as a photocathode. Cu mesh was selected as the base material for the photocathode based on the following considerations: (1) it is a conductive substrate; (2) it can serve as a precursor of Cu<sub>2</sub>O NWA directly; (3) the unique open area of the mesh benefits the flow of electrolyte, and the mesh structure provides extra lateral surface in comparison to a Cu sheet/foil.<sup>36,37</sup> The Cu mesh (100 mesh with the wire diameter being 0.11 mm, Figure S1 in Supporting Information) was first electrochemically anodized with a galvanometric model in 3 M NaOH aqueous solution (Scheme 1a). The galvanometric anodization curve, with a constant current density of 10 mA cm<sup>-2</sup>, is presented in Figure S2. Under these anodization conditions, uniform Cu(OH)<sub>2</sub> NWAs were formed on the Cu mesh surface (Scheme 1b and I). Although CuO is a p-type semiconductor, unlike Cu<sub>2</sub>O, it cannot be employed as photocathodes for hydrogenation because its conduction band edge is more positive than the H<sup>+</sup>/H<sub>2</sub> reduction potential, and H<sub>2</sub> formation is therefore thermodynamically unfavorable.<sup>38,39</sup> In view of the desirable 1-D NWA structure, it is imperative to maintain the NWA architecture of the anodized Cu(OH)<sub>2</sub>/Cu mesh while converting it to Cu<sub>2</sub>O. In the current synthesis, a solution-based glucose coating of the Cu(OH)<sub>2</sub> NWAs/Cu mesh (Scheme 1c and II) and subsequent annealing of the glucose/Cu(OH)<sub>2</sub> NWAs/Cu mesh under inert environment (Scheme 1d) was applied to achieve the delicate conversion of the Cu(OH)<sub>2</sub> to Cu<sub>2</sub>O along with the simultaneous formation of a thin carbon film as a protective layer (Scheme 1e and III). In more detail, the anodized Cu(OH)<sub>2</sub> NWAs/Cu mesh was first soaked into an aqueous glucose solution, dried at ambient condition, and then annealed at 550 °C in N<sub>2</sub> atmosphere to form carbon-layer-coated Cu<sub>2</sub>O NWAs. The concentration of the glucose solution



**Scheme 1.** Photocathode design and synthesis strategy of C/Cu<sub>2</sub>O NWAs/Cu mesh: (a) electrochemical anodization of Cu mesh in 3 M NaOH solution; (b) Cu(OH)<sub>2</sub> NWAs on the Cu mesh; (c) glucose coating on the Cu(OH)<sub>2</sub> NWAs; (d) carbonization of the glucose; (e) carbon-layer-protected Cu<sub>2</sub>O NWAs. (I) Cu(OH)<sub>2</sub> NW; (II) glucose layer on the Cu(OH)<sub>2</sub> NW surface; and (III) carbon-layer-protected Cu<sub>2</sub>O NW.

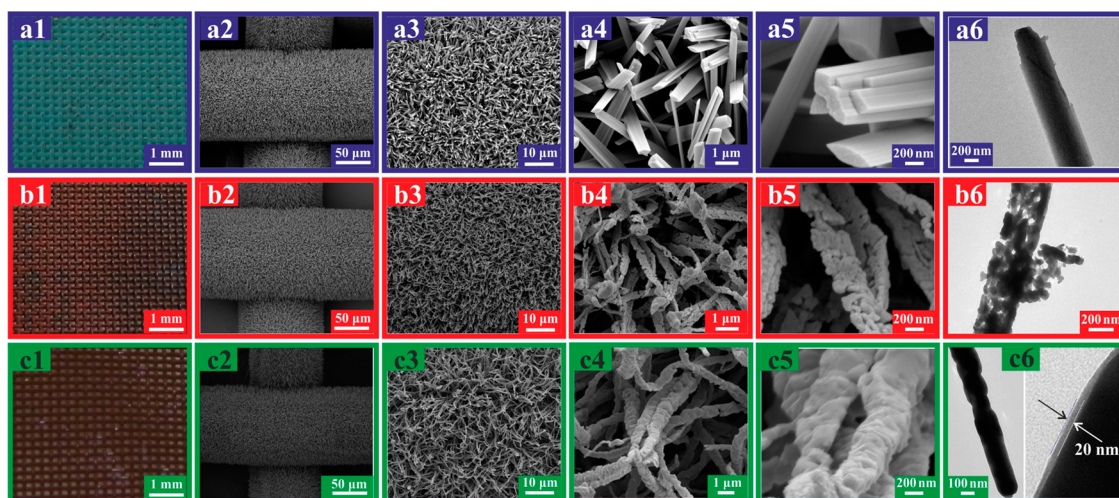


**Figure 1.** Digital photographs, scanning electron microscopy, and transmission electron microscopy images of the Cu(OH)<sub>2</sub> NWAs/Cu mesh (a1–a6); Cu<sub>2</sub>O NWAs/Cu mesh (b1–b6); and C-3-/Cu<sub>2</sub>O NWAs/Cu mesh (c1–c6).

was varied to control the thickness of the final carbon layer on the Cu<sub>2</sub>O NWAs. For the convenience of discussion, we denote the carbon-layer-coated Cu<sub>2</sub>O NWAs/Cu mesh samples with C-x-/Cu<sub>2</sub>O NWAs/Cu mesh, where x represents the glucose solution concentration (mg mL<sup>-1</sup>). The conversion of Cu(OH)<sub>2</sub> to Cu<sub>2</sub>O is presumably achieved by dehydration of Cu(OH)<sub>2</sub> to CuO, followed by removal of oxygen from the lattice of CuO to form Cu<sub>2</sub>O at high temperature in inert N<sub>2</sub> atmosphere.<sup>40,41</sup> At the early stage of the annealing, the glucose dehydrates and cross-links, and as the reaction continues, aromatization and carbonization take place, resulting in a firm carbonized shell covering the NW surfaces, which protects and guarantees the integrity of the original morphology of the starting Cu(OH)<sub>2</sub> NWAs.<sup>42</sup>

This synthesis procedure is simple and facile and, due to its solution-based carbon precursor coating process, it can be employed to nanostructures with other morphologies, as well. The rationally designed

and synthesized C/Cu<sub>2</sub>O NWAs/Cu mesh is expected to work as an efficient and stable photocathode for water splitting application because (1) the Cu<sub>2</sub>O NWAs with a high surface area provide more contact with electrolyte; (2) their high aspect ratio facilitates carrier diffusion; (3) the carbon layer (Scheme 1 III) serves as a protective film, preventing the electrolyte from contacting Cu<sub>2</sub>O NWAs; and (4) the carbon layer also inhibits electron hole recombination,<sup>43,44</sup> facilitating electron transfer into the electrolyte solution where H<sub>2</sub> is generated.

Figure 1a–c presents the digital photographs, scanning electron microscopy (SEM), and transmission electron microscopy (TEM) images of the Cu(OH)<sub>2</sub> NWAs/Cu mesh, Cu<sub>2</sub>O NWAs/Cu mesh without carbon layer, and C-3-/Cu<sub>2</sub>O NWAs/Cu mesh. The digital photograph of the Cu(OH)<sub>2</sub> NWAs/Cu mesh (Figure 1a1) showed a blue color, which agrees well with the typical color of Cu(OH)<sub>2</sub>. Both X-ray diffraction (XRD) (Figure S3) and X-ray photoelectron spectroscopy (XPS) (Figure S4) measurements also confirmed the pure Cu(OH)<sub>2</sub> phase,

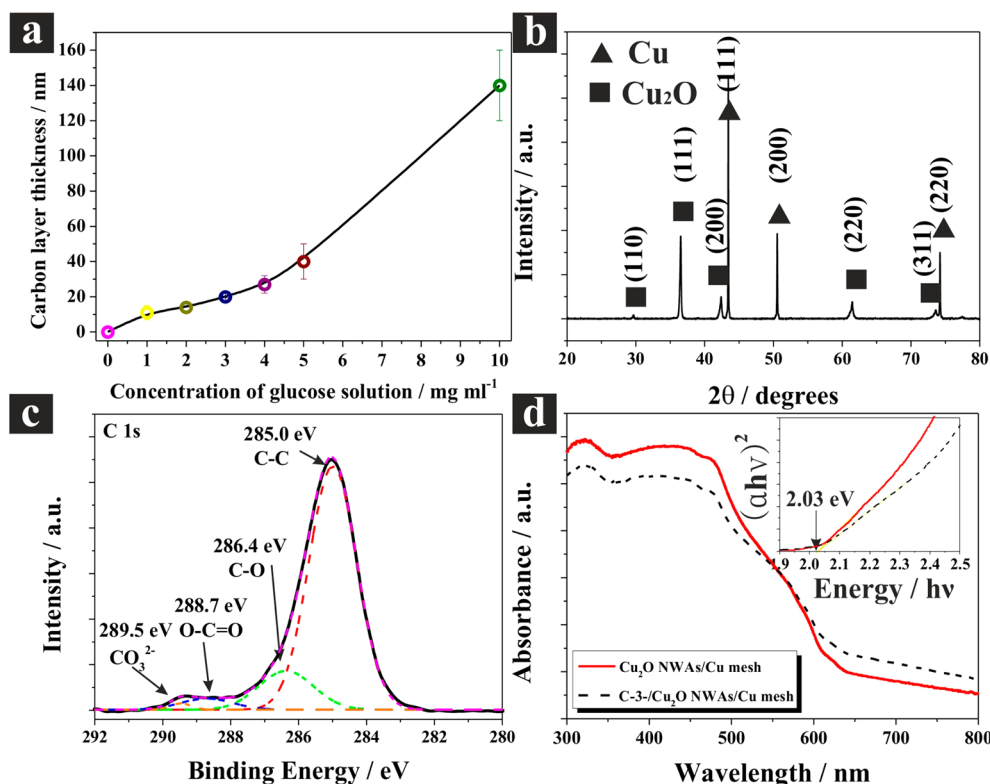


**Figure 2.** (a) Relationship of the glucose concentrations with the average carbon layer thickness of the C-x-/Cu<sub>2</sub>O NWAs/Cu mesh samples. (b) XRD pattern of the C-3-/Cu<sub>2</sub>O NWAs/Cu mesh. (c) XPS core level of C 1s of the C-3-/Cu<sub>2</sub>O NWAs/Cu mesh. (d) UV-visible diffuse reflectance spectra (DRS) of the Cu<sub>2</sub>O NWAs/Cu mesh and C-3-/Cu<sub>2</sub>O NWAs/Cu mesh; the inset shows the plots of transformed Kubelka–Munk function of these two samples versus the energy of light.

with no Cu<sub>2</sub>O and CuO being identified. The SEM images in Figure 1a2–a5 show that the Cu mesh substrate was uniformly covered with a dense layer of the Cu(OH)<sub>2</sub> NWAs. Annealing the naked (*i.e.*, nonprotected) Cu(OH)<sub>2</sub> NWAs/Cu mesh in N<sub>2</sub> atmosphere at 550 °C converted it to Cu<sub>2</sub>O NWAs/Cu mesh, which showed a shiny red color (Figure 1b1), while for the glucose/Cu(OH)<sub>2</sub> NWAs/Cu mesh (Scheme 1II), the annealing under otherwise the same conditions produced C-x-/Cu<sub>2</sub>O NWAs/Cu mesh, which showed a dark red color as exemplified by the C-3-/Cu<sub>2</sub>O NWAs/Cu mesh (Figure 1c1).

The SEM images (Figure 1c2–c5) and TEM image (Figure 1c6) of the C-3-/Cu<sub>2</sub>O NWAs/Cu mesh clearly show that there were no significant morphological changes, and the NWA structure remained during the annealing process. More importantly, the C-3-/Cu<sub>2</sub>O NWAs/Cu mesh showed smooth surfaces with no obvious fractures (Figure 1c6), which stood in a sharp contrast with the Cu<sub>2</sub>O NWAs/Cu mesh whose images showed abundant presence of isolated fractures (Figure 1b4–b6), which would be very undesirable for PEC application of Cu<sub>2</sub>O given its already high tendency toward photocorrosion. The comparison implies that the carbon layer helps to keep the integrity of NWAs during the annealing presumably due to the high strength of the carbon layer. The cross-sectional SEM image of the C-3-/Cu<sub>2</sub>O NWAs/Cu mesh in Figure S5 reveals that the length of the Cu<sub>2</sub>O NWs was around 7–10 μm, which is close the Cu<sub>2</sub>O's

maximum light absorption depth near the band gap (approximately 10 μm),<sup>24,45</sup> and thus guarantees an efficient light absorption. As mentioned previously, the thickness of the carbon layer of the C-x-/Cu<sub>2</sub>O NWAs/Cu mesh can be easily tuned simply by varying the starting glucose concentration. A series of the C-x-/Cu<sub>2</sub>O NWAs/Cu mesh samples were prepared with different glucose concentrations (*i.e.*, 1, 2, 3, 4, 5, 10 mg mL<sup>-1</sup>), and clearly, all of the C-x-/Cu<sub>2</sub>O NWAs/Cu mesh samples showed much better integrity of the original NWA structure than non-carbon-protected Cu<sub>2</sub>O NWAs/Cu mesh (Figure 1 and Figure S6).

It is noted that the C-x-/Cu<sub>2</sub>O NWAs/Cu mesh samples prepared at low glucose concentrations (*i.e.*, 1 and 2 mg mL<sup>-1</sup>) showed some fractures on the carbon surfaces (Figure S6a,b), while any further increase of the glucose concentration beyond 2 mg mL<sup>-1</sup> led to continuous carbon coatings on the NWAs' surfaces with no fractures visible (Figure 1c and Figure S6c–e). These results suggest that the minimum glucose concentration for forming a continuous carbon coating layer in the current system is 3.0 mg mL<sup>-1</sup>. The relationship between the glucose concentrations and average carbon layer thickness, calculated based on the TEM measurements, is summarized in Figure 2a, which clearly shows that the average carbon layer thickness increased with increasing glucose concentration, in an almost linear manner.

Figure 2b shows the XRD pattern of the C-3-/Cu<sub>2</sub>O NWAs/Cu mesh. As can be seen, besides three peaks for elemental Cu coming from the Cu mesh substrate, others are all attributed to Cu<sub>2</sub>O phase with a strong (111) orientation, without CuO or Cu(OH)<sub>2</sub> being identified.<sup>46</sup> The XPS of C 1s core level for the C-3-/Cu<sub>2</sub>O NWAs/Cu mesh sample is presented in Figure 2c. The experimental curves were well fitted with a Gauss peaks model after Shirley background subtraction. The strong C–C peak at 285.0 eV implies the formation of a carbon layer on the Cu<sub>2</sub>O NWA surface, while the much lower intensities of C–O, O–C=O, and CO<sub>3</sub><sup>2-</sup> peaks are attributed to the left over oxygen functional groups within the carbon layer.<sup>47,48</sup> From XPS measurement, no evidence was observed for the formation of a Cu–C bond, and elemental Cu was not detected in the NWAs (Figure S7).<sup>49,50</sup>

The optical properties of the Cu<sub>2</sub>O NWAs/Cu mesh and C-3-/Cu<sub>2</sub>O NWAs/Cu mesh were measured using UV-vis diffuse reflectance spectra (DRS) and are presented in Figure 2d. Compared with the Cu<sub>2</sub>O NWAs/Cu mesh (red solid line in Figure 2d), the C-3-/Cu<sub>2</sub>O NWAs/Cu mesh (black dashed line in Figure 2d) showed an enhanced absorption in the long wavelength region ranging from 600 to 800 nm, which is due to the strong absorption of the carbon layer in this region and which agrees well with the color change of the samples (Figure 1b1,c1). However, a decreased absorption in the short wavelength region ranging from 300 to 600 nm was also observed, which implies that the carbon layer reduces the optical absorption of the Cu<sub>2</sub>O NWAs to some extent within this range. This phenomenon was observed on all C-x-/Cu<sub>2</sub>O NWAs/Cu mesh samples prepared in this study, with thicker carbon layers leading to higher reduction in optical absorption of the Cu<sub>2</sub>O NWAs within the short wavelength region, to which Cu<sub>2</sub>O is photocatalytically responsive due to its band gap (Figure S8). Thus, from a combined viewpoint of lower light absorption (in short wavelength region) for thicker carbon coatings and surface fractures for thinner carbon coatings, there seems to exist an optimal carbon thickness which would give maximum PEC performance for such a carbon-layer-coated Cu<sub>2</sub>O NWA photoelectrode.

The DRS measurements were transformed using the Kubelka–Munk function and plotted against the energy of light (inset in Figure 2d),<sup>51,52</sup> from which the same band gap values of 2.03 eV for the Cu<sub>2</sub>O NWAs/Cu mesh and C-3-/Cu<sub>2</sub>O NWAs/Cu mesh were estimated, indicating that no band gap narrowing occurred with the carbon layer coating and thus implying that there was no carbon elements doped into the Cu<sub>2</sub>O lattice. The results agree well with the results from the XPS measurement.

To evaluate the PEC performances of the Cu<sub>2</sub>O NWAs/Cu mesh and C-x-/Cu<sub>2</sub>O NWAs/Cu mesh photocathodes, linear sweep voltammetry (LSV) measurements

were performed in 1 M Na<sub>2</sub>SO<sub>4</sub> electrolyte under AM 1.5G (100 mW cm<sup>-2</sup>) illumination using a three-electrode electrochemical system, with the Cu-mesh-based photoelectrode, Ag/AgCl electrode, and Pt mesh as working electrode, reference electrode, and counter electrode, respectively. During the LSV scan, the illumination was chopped with a frequency of 0.2 Hz so that the dark and the light currents could be simultaneously monitored. It is worth mentioning that, in the field of water splitting, the photocurrent going through an external circuit is widely used as a reliable surrogate for hydrogen and oxygen gas measurement in evaluating the performance of various semiconductors, including Cu<sub>2</sub>O.<sup>30,53–56</sup> The results show that the C-3-/Cu<sub>2</sub>O NWAs/Cu mesh photocathode generated a photocurrent density of  $-3.95 \text{ mA cm}^{-2}$  (Figure 3a1) at 0 V vs reversible hydrogen electrode (RHE) (the potential often chosen as a metric to evaluate the performance of photocathode as it corresponds to the water reduction potential),<sup>31,57,58</sup> which is the highest among all samples tested in this work. To the best of our knowledge, this value is the highest ever reported for Cu<sub>2</sub>O materials without the use of any cocatalyst,<sup>33,59</sup> and it is much higher than  $-2.28 \text{ mA cm}^{-2}$  generated on the bare Cu<sub>2</sub>O NWAs/Cu mesh (Figure 3b1). A digital photo of hydrogen gas bubbles generated on the C-3-/Cu<sub>2</sub>O NWAs/Cu mesh photocathode is presented in Figure S9. A possible mechanism for the improved photocurrent density on the C-3-/Cu<sub>2</sub>O NWAs/Cu mesh photocathode will be presented in a later section.

The photoconversion efficiencies of the Cu<sub>2</sub>O NWAs/Cu mesh and C-3-/Cu<sub>2</sub>O NWAs/Cu mesh photocathodes were calculated with the equation of  $\eta = J_{\text{Pmax}} V_{\text{Pmax}} / P_{\text{in}}$ ,<sup>3,60,61</sup> where  $J_{\text{Pmax}}$  and  $V_{\text{Pmax}}$  are the current density ( $\text{mW cm}^{-2}$ ) and photovoltage (V vs RHE) at the maximum power point and  $P_{\text{in}}$  ( $\text{mW cm}^{-2}$ ) is the incoming light flux (100  $\text{mW cm}^{-2}$  in our case). The insets in Figure 3a1,b1 present the plots of the photoconversion efficiencies versus applied bias potentials for the Cu<sub>2</sub>O NWAs/Cu mesh and C-3-/Cu<sub>2</sub>O NWAs/Cu mesh photocathodes, respectively. The Cu<sub>2</sub>O NWAs/Cu mesh exhibited an optimal conversion efficiency of 0.28%, while the C-3-/Cu<sub>2</sub>O NWAs/Cu mesh achieved a much higher optimal conversion efficiency of 0.56% at the potential of 0.21 V vs RHE.

The PEC performances of all C-x-/Cu<sub>2</sub>O NWAs/Cu mesh samples are presented in Figure S10 and summarized in Figure 4. The photocurrent densities of the C-x-/Cu<sub>2</sub>O NWAs/Cu mesh first increased with increasing glucose concentrations and thus with increasing carbon layer thickness and reached a peak at the glucose concentration at 3 mg mL<sup>-1</sup> and at correspondingly at a carbon layer thickness of 20 nm (i.e., C-3-/Cu<sub>2</sub>O NWAs/Cu mesh) before declining monotonically thereafter. The deteriorating PEC performance on the C-x-/Cu<sub>2</sub>O NWAs/Cu mesh samples with thicker carbon layer can be ascribed to a stronger optical

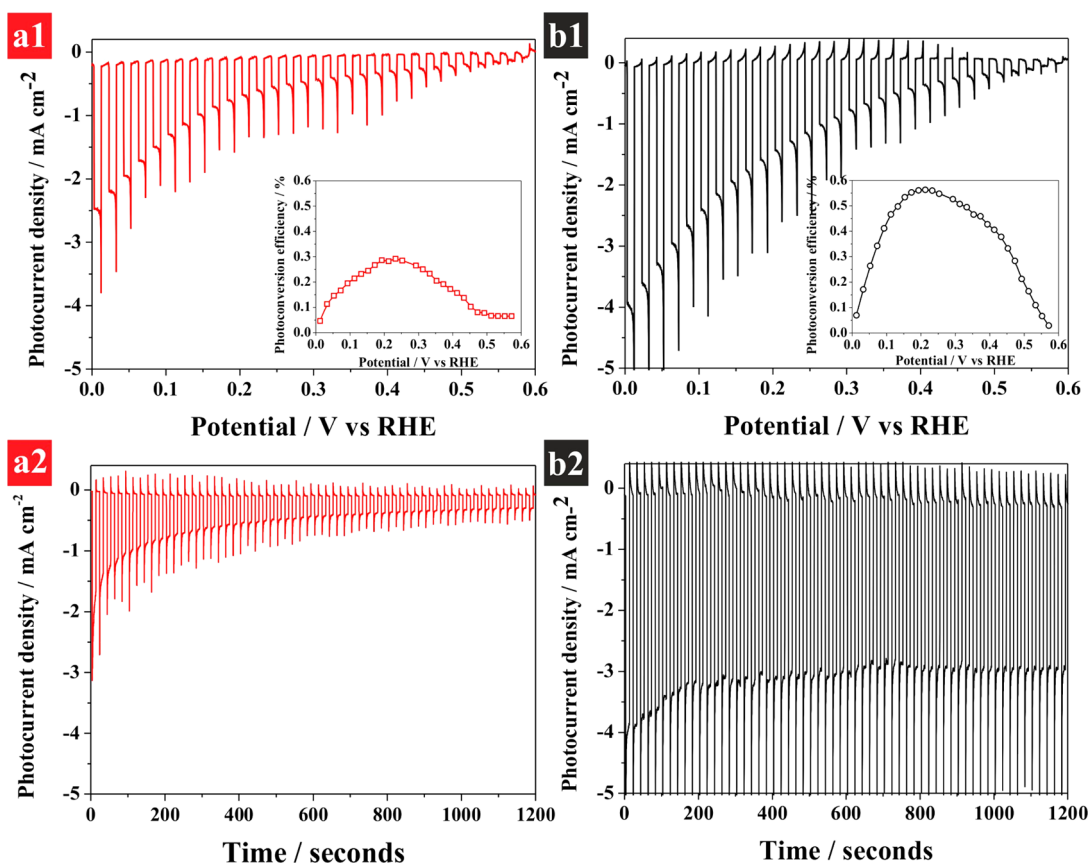


**Figure 3.** Photoelectrochemical performance of (a1) the Cu<sub>2</sub>O NWAs/Cu mesh and (b1) C-3-/Cu<sub>2</sub>O NWAs/Cu mesh under illumination of chopped AM 1.5G (light on/off cycle: 5 s); insets in (a1) and (b1) plotted the photoconversion efficiencies vs applied bias potentials for Cu<sub>2</sub>O NWAs/Cu mesh and C-3-/Cu<sub>2</sub>O NWAs/Cu mesh, respectively, and respective photocurrent density decay at 0 V vs RHE in chopped light illumination (light on/off cycle: 10 s) for stability evaluation (a2,b2).

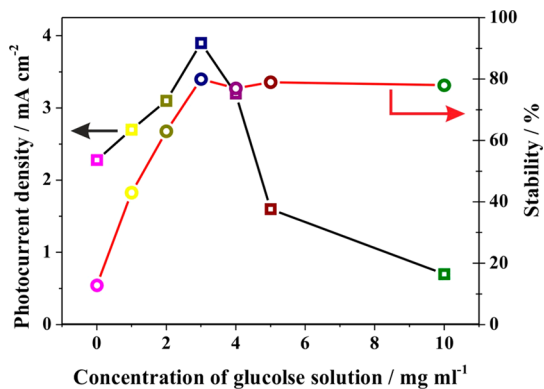


**Figure 4.** Photocurrent densities (measured at 0 V vs RHE) and photostability of the C-x-/Cu<sub>2</sub>O NWAs/Cu mesh photoelectrodes as a function of glucose concentration and thus carbon layer thickness.

blocking by the carbon layers, which reduces the light absorption of the Cu<sub>2</sub>O NWAs within the wavelength range between 300 and 600 nm, as discussed earlier.

To further illustrate the merits of the 1-D nanostructure, non-one-dimensional and large-sized Cu<sub>2</sub>O crystal structures (SEM images in Figure S11) were also synthesized directly on the Cu meshes at relatively low anodization current densities (0.2–5.0 mA cm<sup>-2</sup>), and

the PEC performances of these samples were evaluated under otherwise the same conditions and are presented in Figure S12. It turns out that the photocurrent densities of these non-one-dimensional samples were measured only to be in a range of −0.1 to −1.04 mA cm<sup>-2</sup>, much lower than these on the NWA-based Cu<sub>2</sub>O samples, namely, the Cu<sub>2</sub>O NWAs/Cu mesh and C/Cu<sub>2</sub>O NWAs/Cu mesh, which can be ascribed to the higher surface area and facilitated charge carrier diffusion with the one-dimensional nanostructures.

The stability of the photocathodes under illumination was evaluated with chronoamperometric measurements at 0 V vs RHE in chopped light with the same intensity and with a frequency of 0.1 Hz over 20 min, a condition which is widely used as a semi-standard for comparing photostability of a semiconductor.<sup>21,32,33</sup> The photostability was quantified as the percentage of the photocurrent density at the end of the last light cycle ( $J$ ) compared with that at the end of the first light cycle ( $J_0$ ) within the 20 min measurement period.<sup>17,21,32,33</sup> As shown in Figure 4 and Figure S10, all C-x-/Cu<sub>2</sub>O NWAs/Cu mesh samples exhibited considerably improved photostability, increasing almost linearly with the carbon layer thickness before reaching a plateau at 80.7% with a carbon layer thickness of 20 nm

(i.e., C-3-/Cu<sub>2</sub>O NWAs/Cu mesh). A close comparison of the photocurrent density decay curves of the C-3-/Cu<sub>2</sub>O NWAs/Cu mesh and Cu<sub>2</sub>O NWAs/Cu mesh photocathodes is presented in Figure 3a2,b2. Compared with the photostability of only 12.6% for the non-carbon-protected Cu<sub>2</sub>O NWAs/Cu mesh photocathode, the C-3-/Cu<sub>2</sub>O NWAs/Cu mesh photocathode showed a remarkably improved photostability of 80.7% (almost 600% increase). This demonstrates the protective role of the carbon layer coating and thus exemplifies that the carbon layer protection strategy is indeed an effective strategy for combating the photocorrosion problem of unstable semiconductors. The photostability measurement was also performed for a longer period of time (i.e., 1 h), and the results are presented in Figure S13. As can be seen, after 1 h illumination, the Cu<sub>2</sub>O NWAs/Cu mesh almost lost its photoactivity completely, while the C-3-/Cu<sub>2</sub>O NWAs/Cu mesh maintained 75% of its original photoactivity. Furthermore, the SEM images of the Cu<sub>2</sub>O NWAs/Cu mesh and C-3-/Cu<sub>2</sub>O NWAs/Cu mesh after 1 h illumination are presented in Figure S14, and clearly, some metallic copper particles were found on the surface of the Cu<sub>2</sub>O NWAs/Cu mesh sample, but no copper particles could be identified on the C-3-/Cu<sub>2</sub>O NWAs/Cu mesh sample, which partially confirms the enhanced photostability with the carbon protective layer.

Increasing the carbon layer thickness beyond 20 nm did not result in any further improvement in photoelectrodes' photostability, and thus an optimal carbon thickness of 20 nm was identified in the current study (C-3-/Cu<sub>2</sub>O NWAs/Cu mesh), and since among all of the samples tested in this study, the C-3-/Cu<sub>2</sub>O NWAs/Cu mesh gave the highest photocurrent density, as well, it is the optimal photoelectrode for water splitting application. Furthermore, not surprisingly, all of the non-one-dimensional and non-carbon-protected Cu<sub>2</sub>O/Cu mesh samples showed very low photostability, less than 10% (Figure S12).

The electrochemical impedance spectroscopy (EIS) is a powerful tool for studying a material's PEC properties.<sup>62</sup> The EIS measurement was carried out covering the frequency of 10<sup>5</sup>–0.1 Hz interval using an

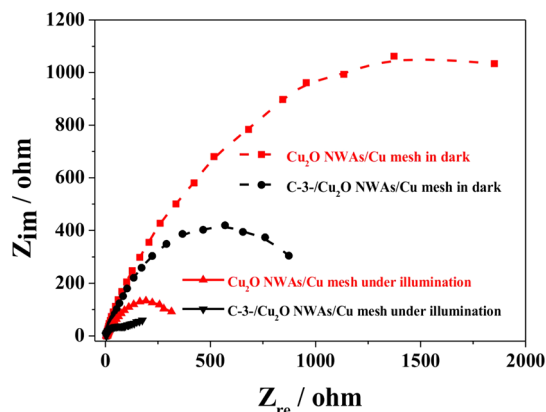


**Figure 5.** Nyquist plots ( $Z_{\text{re}}$  vs  $Z_{\text{im}}$ ) for the Cu<sub>2</sub>O NWAs/Cu mesh and C-3-/Cu<sub>2</sub>O NWAs/Cu mesh photocathodes in dark and under illumination.

amplitude of 10 mV at a bias potential of 0 V vs RHE. Figure 5 presents Nyquist plots for the Cu<sub>2</sub>O NWAs/Cu mesh and C-3-/Cu<sub>2</sub>O NWAs/Cu mesh in dark and under illumination. It is known that the semicircle in a Nyquist plot at high frequencies is characteristic of the charge transfer process and the diameter of the semicircle is equal to the charge transfer resistance ( $R_{\text{ct}}$ ).<sup>63</sup> The C-3-/Cu<sub>2</sub>O NWAs/Cu mesh showed a lower  $R_{\text{ct}}$  value than the Cu<sub>2</sub>O NWAs/Cu mesh both in dark and under illumination, which is presumably due to the good conductivity of the carbon layer on the Cu<sub>2</sub>O nanowire surface. The carbon layer thus facilitates the electron transfer from Cu<sub>2</sub>O to the electrolyte, resulting in an overall reduced charge transfer resistance, which also explains the better PEC performance of the C-x-/Cu<sub>2</sub>O NWAs/Cu mesh.

## CONCLUSION

In this work, a facile strategy based on coating a thin protective carbon layer was proposed to combat the photocorrosion problem of unstable semiconductors. The proof-of-concept test successfully showed that the thin carbon-layer-protected Cu<sub>2</sub>O nanowire arrays not only exhibited remarkably improved photostability but also showed significantly improved water splitting performance.

## EXPERIMENTAL SECTION

**Preparation of C-x-/Cu NWAs/Cu Mesh Photocathode.** The Cu mesh (Alfa Aesar, 100 mesh, 0.11 mm as wire diameter) was anodized in an alkali solution (3 M NaOH) for 30 min under 10 mA cm<sup>-2</sup> to form Cu(OH)<sub>2</sub> NWAs/Cu mesh. The Cu<sub>2</sub>O crystals with large size were synthesized under different current densities ranging from 0.2 to 5 mA cm<sup>-2</sup>. The temperature of the electrochemical cells was maintained at 25 °C for all experiments. The as-anodized Cu(OH)<sub>2</sub> NWAs/Cu mesh was annealed at 550 °C at N<sub>2</sub> atmosphere for 4 h with or without glucose coating. The glucose solution was prepared using deionized water only.

**Structural Characterization.** The morphologies of the C-x-/Cu NWAs/Cu mesh photocathodes were characterized by scanning

electron microscopy (SEM, FEI, Quanta 600) and transmission electron microscope (TEM, Tecnai T12). The crystalline structure of the samples was analyzed by X-ray diffraction (XRD) (Bruker D8 Discover diffractometer, using Cu K $\alpha$  radiation (1.540598 Å)). The chemical compositions and status were analyzed by X-ray photoelectron spectroscopy (XPS) with an Axis Ultra instrument (Kratos Analytical) under ultrahigh vacuum (<10<sup>-8</sup> Torr) and by using a monochromatic Al K $\alpha$  X-ray source. The adventitious carbon 1s peak was calibrated at 285 eV and used as an internal standard to compensate for any charging effects. The diffuse reflectance UV-vis adsorption spectra were recorded on spectrophotometer (Shimadzu, UV 2550), with fine BaSO<sub>4</sub> powder as reference. All digital photos were taken by a Cannon EOS 7D.

**Photoelectrochemical Measurements.** The PEC performance of the prepared C-x-/Cu NWAs/Cu mesh photocathodes was evaluated using a three-electrode configuration with C-x-/Cu NWAs/Cu mesh, Ag/AgCl, and Pt gauze as working electrodes, reference electrode, and counter electrode, respectively. The electrolyte used was 1.0 M Na<sub>2</sub>SO<sub>4</sub> solution. The photoresponse of the prepared photoelectrodes was measured under a chopped irradiation from a 300 W Xe lamp (PLS-SXE300) (light on/off cycle: 5 s). The intensity of light source was calibrated with a Si diode (Newport) to simulate AM 1.5 illumination (100 mW cm<sup>-2</sup>). The scan rate for the linear sweep voltammetry was 2 mV s<sup>-1</sup>. The PEC stability of the materials was evaluated by measuring the photocurrent densities produced under chopped light irradiation (light on/off cycles: 10 s) at a fixed electrode potential of 0 V vs RHE. The impedance measurements were performed using a PGSTAT302N Autolab potentiostat/galvanostat (Metrohm) equipped with a frequency analyzer module (FRA2). The electrochemical impedance spectra were done at an excitation signal of 10 mV amplitude. The impedance versus frequency spectra were acquired at fixed sample potentials. Afterward, impedance versus potential measurement at fixed frequencies of 5 kHz was performed.

**Conflict of Interest:** The authors declare no competing financial interest.

**Acknowledgment.** The authors are grateful to KAUST for providing very generous financial support. We thank Prof. Micheal Grätzel for valuable discussion on photoconversion efficiency calculation.

**Supporting Information Available:** SEM, TEM, XRD, XPS, DRS, and PEC performances of other samples. This material is available free of charge via the Internet at <http://pubs.acs.org>.

## REFERENCES AND NOTES

- Fujishima, A.; Honda, K. Electrochemical Photolysis of Water at a Semiconductor Electrode. *Nature* **1972**, *238*, 37–38.
- Grätzel, M. Photoelectrochemical Cells. *Nature* **2001**, *414*, 338–344.
- Walter, M. G.; Warren, E. L.; McKone, J. R.; Boettcher, S. W.; Mi, Q.; Santori, E. A.; Lewis, N. S. Solar Water Splitting Cells. *Chem. Rev.* **2010**, *110*, 6446–6473.
- Chen, C. Y.; Retamal, J. R. D.; Wu, I. W.; Lien, D. H.; Chen, M. W.; Ding, Y.; Chueh, Y. L.; Wu, C. I.; He, J. H. Probing Surface Band Bending of Surface-Engineered Metal Oxide Nanowires. *ACS Nano* **2012**, *6*, 9366–9372.
- Zhang, Z.; Yates, J. T., Jr. Band Bending in Semiconductors: Chemical and Physical Consequences at Surfaces and Interfaces. *Chem. Rev.* **2012**, *112*, 5520–5551.
- Lin, Y.; Zhou, S.; Liu, X.; Sheehan, S.; Wang, D. TiO<sub>2</sub>/TiSi<sub>2</sub> Heterostructures for High-Efficiency Photoelectrochemical H<sub>2</sub>O Splitting. *J. Am. Chem. Soc.* **2009**, *131*, 2772–2773.
- Liu, C.; Sun, J.; Tang, J.; Yang, P. Zn-Doped p-Type Gallium Phosphide Nanowire Photocathodes from a Surfactant-Free Solution Synthesis. *Nano Lett.* **2012**, *12*, 5407–5411.
- Aryal, K.; Pantha, B. N.; Li, J.; Lin, J. Y.; Jiang, H. X. Hydrogen Generation by Solar Water Splitting Using p-InGaN Photoelectrochemical Cells. *Appl. Phys. Lett.* **2010**, *96*, 052110–052113.
- Li, L.; Duan, L.; Wen, F.; Li, C.; Wang, M.; Hagfeldt, A.; Sun, L. Visible Light Driven Hydrogen Production from a Photoactive Cathode Based on a Molecular Catalyst and Organic Dye-Sensitized p-Type Nanostructured NiO. *Chem. Commun.* **2012**, *48*, 988–990.
- Xiong, L.; Huang, S.; Yang, X.; Qiu, M.; Chen, Z.; Yu, Y. p-Type and n-Type Cu<sub>2</sub>O Semiconductor Thin Films: Controllable Preparation by Simple Solvothermal Method and Photoelectrochemical Properties. *Electrochim. Acta* **2011**, *56*, 2735–2739.
- Chen, X.; Shen, S.; Guo, L.; Mao, S. S. Semiconductor-Based Photocatalytic Hydrogen Generation. *Chem. Rev.* **2010**, *110*, 6503–6570.
- Zhang, Z.; Wang, P. Optimization of Photoelectrochemical Water Splitting Performance on Hierarchical TiO<sub>2</sub> Nanotube Arrays. *Energy Environ. Sci.* **2012**, *5*, 6506–6512.
- Wang, X.; Zhu, H.; Xu, Y.; Wang, H.; Tao, Y.; Hark, S.; Xiao, X.; Li, Q. Aligned ZnO/CdTe Core–Shell Nanocable Arrays on Indium Tin Oxide: Synthesis and Photoelectrochemical Properties. *ACS Nano* **2010**, *4*, 3302–3308.
- Hahn, N. T.; Ye, H.; Flaherty, D. W.; Bard, A. J.; Mullins, C. B. Reactive Ballistic Deposition of α-Fe<sub>2</sub>O<sub>3</sub> Thin Films for Photoelectrochemical Water Oxidation. *ACS Nano* **2010**, *4*, 1977–1986.
- Liu, X.; Wang, F.; Wang, Q. Nanostructure-Based WO<sub>3</sub> Photoanodes for Photoelectrochemical Water Splitting. *Phys. Chem. Chem. Phys.* **2012**, *14*, 7894–7911.
- Chen, X.; Ye, J.; Ouyang, S.; Kako, T.; Li, Z.; Zou, Z. Enhanced Incident Photo-to-Electron Conversion Efficiency of Tungsten Trioxide Photoanodes Based on 3D-Photonic Crystal Design. *ACS Nano* **2011**, *5*, 4310–4318.
- Paracchino, A.; Brauer, J. C.; Moser, J. E.; Thimsen, E.; Grätzel, M. Synthesis and Characterization of High-Photoactivity Electrodeposited Cu<sub>2</sub>O Solar Absorber by Photoelectrochemistry and Ultrafast Spectroscopy. *J. Phys. Chem. C* **2012**, *116*, 7341–7350.
- Mahmoud, M. A.; Qian, W.; El-Sayed, M. A. Following Charge Separation on the Nanoscale in Cu<sub>2</sub>O-Au Nanoframe Hollow Nanoparticles. *Nano Lett.* **2011**, *11*, 3285–3289.
- Radi, A.; Pradhan, D.; Sohn, Y.; Leung, K. Nanoscale Shape and Size Control of Cubic, Cubooctahedral, and Octahedral Cu-Cu<sub>2</sub>O Core–Shell Nanoparticles on Si(100) by One-Step, Templateless, Capping-Agent-Free Electrodeposition. *ACS Nano* **2010**, *4*, 1553–1560.
- de Jongh, P. E.; Vanmaekelbergh, D.; Kelly, J. J. Photoelectrochemistry of Electrodeposited Cu<sub>2</sub>O. *J. Electrochem. Soc.* **2000**, *147*, 486–489.
- Paracchino, A.; Laporte, V.; Sivila, K.; Grätzel, M.; Thimsen, E. Highly Active Oxide Photocathode for Photoelectrochemical Water Reduction. *Nat. Mater.* **2011**, *10*, 456–461.
- Halicioglu, S.; Meng, F.; Jin, S. Facile and Mild Solution Synthesis of Cu<sub>2</sub>O Nanowires and Nanotubes Driven by Screw Dislocations. *Chem. Commun.* **2012**, *48*, 1174–1176.
- de Jongh, P. E.; Vanmaekelbergh, D.; Kelly, J. J. Cu<sub>2</sub>O: Electrodeposition and Characterization. *Chem. Mater.* **1999**, *11*, 3512–3517.
- Engel, C. J.; Polson, T. A.; Spado, J. R.; Bell, J. M.; Fillinger, A. Photoelectrochemistry of Porous p-Cu<sub>2</sub>O Films. *J. Electrochem. Soc.* **2008**, *155*, F37–F42.
- Gerischer, H. On the Stability of Semiconductor Electrodes against Photodecomposition. *J. Electroanal. Chem.* **1977**, *82*, 133–143.
- Zhang, Z.; Zhang, L.; Hedhili, M. N.; Zhang, H.; Wang, P. Plasmonic Gold Nanocrystals Coupled with Photonic Crystal Seamlessly on TiO<sub>2</sub> Nanotube Photoelectrodes for Efficient Visible Light Photoelectrochemical Water Splitting. *Nano Lett.* **2013**, *13*, 14–20.
- Zhang, J.; Bang, J. H.; Tang, C.; Kamat, P. V. Tailored TiO<sub>2</sub>-SrTiO<sub>3</sub> Heterostructure Nanotube Arrays for Improved Photoelectrochemical Performance. *ACS Nano* **2010**, *4*, 387–395.
- Hwang, Y. J.; Wu, C. H.; Hahn, C.; Jeong, H. E.; Yang, P. Si/InGaN Core/Shell Hierarchical Nanowire Arrays and Their Photoelectrochemical Properties. *Nano Lett.* **2012**, *12*, 1678–1682.
- Boettcher, S. W.; Spurgeon, J. M.; Putnam, M. C.; Warren, E. L.; Turner-Evans, D. B.; Kelzenberg, M. D.; Maiolo, J. R.; Atwater, H. A.; Lewis, N. S. Energy-Conversion Properties of Vapor–Liquid–Solid-Grown Silicon Wire-Array Photocathodes. *Science* **2010**, *327*, 185–187.
- Qian, F.; Wang, G.; Li, Y. Solar-Driven Microbial Photoelectrochemical Cells with a Nanowire Photocathode. *Nano Lett.* **2010**, *10*, 4686–4691.
- Lin, C. Y.; Lai, Y. H.; Mersch, D.; Reisner, E. Cu<sub>2</sub>O|NiO<sub>x</sub> Nanocomposite as an Inexpensive Photocathode in Photoelectrochemical Water Splitting. *Chem. Sci.* **2012**, *3*, 3482–3487.
- Paracchino, A.; Mathews, N.; Hisatomi, T.; Stefk, M.; Tilley, S. D.; Grätzel, M. Ultrathin Films on Copper(I) Oxide Water Splitting Photocathodes: A Study on Performance and Stability. *Energy Environ. Sci.* **2012**, *5*, 8673–8681.

33. Zhang, Z.; Wang, P. Highly Stable Copper Oxide Composites as an Effective Photocathode for Water Splitting *via* a Facile Electrochemical Synthesis Strategy. *J. Mater. Chem.* **2012**, *22*, 2456–2464.
34. Dai, L.; Chang, D. K.; Baek, J. B.; Lu, W. Carbon Nanomaterials for Advanced Energy Conversion and Storage. *Small* **2012**, *8*, 1130–1166.
35. Wang, Y.; Zhang, H. J.; Lu, L.; Stubbs, L. P.; Wong, C. C.; Lin, J. Designed Functional Systems from Peapod-like Co@Carbon to Co<sub>3</sub>O<sub>4</sub>@Carbon Nanocomposites. *ACS Nano* **2010**, *4*, 4753–4761.
36. Liu, Z.; Zhang, Q.; Zhao, T.; Zhai, J.; Jiang, L. 3-D Vertical Arrays of TiO<sub>2</sub> Nanotubes on Ti Mesh: Efficient Photoanodes for Water Photoelectrolysis. *J. Mater. Chem.* **2011**, *21*, 10354–10358.
37. La, D. D.; Nguyen, T. A.; Lee, S.; Kim, J. W.; Kim, Y. S. A Stable Superhydrophobic and Superoleophilic Cu Mesh Based on Copper Hydroxide Nanoneedle Arrays. *Appl. Surf. Sci.* **2011**, *257*, 5705–5710.
38. Mor, G. K.; Varghese, O. K.; Wilke, R. H. T.; Sharma, S.; Shankar, K.; Latempa, T. J.; Choi, K. S.; Grimes, C. A. p-Type Cu-Ti-O Nanotube Arrays and Their Use in Self-Biased Heterojunction Photoelectrochemical Diodes for Hydrogen Generation. *Nano Lett.* **2008**, *8*, 1906–1911.
39. Choi, H. J.; Kang, M. Hydrogen Production from Methanol/Water Decomposition in a Liquid Photosystem Using the Anatase Structure of Cu Loaded TiO<sub>2</sub>. *Int. J. Hydrogen Energy* **2007**, *32*, 3841–3848.
40. Zhang, W.; Wen, X.; Yang, S.; Berta, Y.; Wang, Z. L. Single-Crystalline Scroll-Type Nanotube Arrays of Copper Hydroxide Synthesized at Room Temperature. *Adv. Mater.* **2003**, *15*, 822–825.
41. Lu, C.; Qi, L.; Yang, J.; Zhang, D.; Wu, N.; Ma, J. Simple Template-Free Solution Route for the Controlled Synthesis of Cu(OH)<sub>2</sub> and CuO Nanostructures. *J. Phys. Chem. B* **2004**, *108*, 17825–17831.
42. Li, Z.; Guo, H.; Qian, H.; Hu, Y. Facile Microemulsion Route To Coat Carbonized Glucose on Upconversion Nanocrystals as High Luminescence and Biocompatible Cell-Imaging Probes. *Nanotechnology* **2010**, *21*, 315105–315111.
43. Du, J.; Lai, X.; Yang, N.; Zhai, J.; Kisailius, D.; Su, F.; Wang, D.; Jiang, L. Hierarchical Ordered Macro-Mesoporous TiO<sub>2</sub>-Graphene Composite Films: Improved Mass Transfer, Reduced Charge Recombination, and Their Enhanced Photocatalytic Activities. *ACS Nano* **2011**, *5*, 590–596.
44. Woan, K.; Pyrgiotakis, G.; Sigmund, W. Photocatalytic Carbon-Nanotube-TiO<sub>2</sub> Composites. *Adv. Mater.* **2009**, *21*, 2233–2239.
45. Sculfort, J. L.; Guyomard, D.; Herlem, M. Photoelectrochemical Characterization of the p-Cu<sub>2</sub>O-Nonaqueous Electrolyte Junction. *Electrochim. Acta* **1984**, *29*, 459–465.
46. PDF-2 Database, International Center for Diffraction Data, **2004**.
47. Cano, E.; Torres, C. L.; Bastidas, J. M. An XPS Study of Copper Corrosion Originated by Formic Acid Vapour at 40% and 80% Relative Humidity. *Mater. Corros.* **2001**, *52*, 667–676.
48. Tang, L.; Ji, R.; Cao, X.; Lin, J.; Jiang, H.; Li, X.; Teng, K. S.; Luk, C. M.; Zeng, S.; Hao, J.; et al. Deep Ultraviolet Photoluminescence of Water-Soluble Self-Passivated Graphene Quantum Dots. *ACS Nano* **2012**, *6*, 5102–5110.
49. Fu, R.; Yoshizawa, N.; Dresselhaus, M. S.; Dresselhaus, G.; Satcher, J. H., Jr.; Baumann, T. F. XPS Study of Copper-Doped Carbon Aerogels. *Langmuir* **2002**, *18*, 10100–10104.
50. Akhavan, O.; Azimirad, R.; Safa, S.; Hasani, E. CuO/Cu(OH)<sub>2</sub> Hierarchical Nanostructures as Bactericidal Photocatalysts. *J. Mater. Chem.* **2011**, *21*, 9634–9640.
51. Zhang, Y.; Zhang, N.; Tang, Z. R.; Xu, Y. J. Graphene Transforms Wide Band Gap ZnS to a Visible Light Photocatalyst. The New Role of Graphene as a Macromolecular Photosensitizer. *ACS Nano* **2012**, *6*, 9777–9789.
52. Zhao, W.; Fu, W.; Yang, H.; Tian, C.; Li, M.; Li, Y.; Zhang, L.; Sui, Y.; Zhou, X.; Chen, H.; et al. Electrodeposition of Cu<sub>2</sub>O Films and Their Photoelectrochemical Properties. *CrystEngComm* **2011**, *13*, 2871–2877.
53. Khan, S. U. M.; Al-Shahry, M.; Ingler, W. B., Jr. Efficient Photochemical Water Splitting by a Chemically Modified n-TiO<sub>2</sub>. *Science* **2002**, *297*, 2243–2245.
54. Allam, N. K.; Alamgir, F.; El-Sayed, M. A. Enhanced Photo-assisted Water Electrolysis Using Vertically Oriented Anodically Fabricated Ti-Nb-Zr-O Mixed Oxide Nanotube Arrays. *ACS Nano* **2010**, *4*, 5819–5826.
55. Mayer, M. T.; Du, C.; Wang, D. Hematite/Si Nanowire Dual-Absorber System for Photoelectrochemical Water Splitting at Low Applied Potentials. *J. Am. Chem. Soc.* **2012**, *134*, 12406–12409.
56. Klahr, B.; Gimenez, S.; Fabregat-Santiago, F.; Bisquert, J.; Hamann, T. W. Photoelectrochemical and Impedance Spectroscopic Investigation of Water Oxidation with "Co-Pi"-Coated Hematite Electrodes. *J. Am. Chem. Soc.* **2012**, *134*, 16693–16700.
57. Kim, J.; Minegishi, T.; Kobota, J.; Domen, K. Enhanced Photoelectrochemical Properties of CuGa<sub>3</sub>Se<sub>5</sub> Thin Films for Water Splitting by the Hydrogen Mediated Co-evaporation Method. *Energy Environ. Sci.* **2012**, *5*, 6368–6374.
58. Yokoyama, D.; Minegishi, T.; Maeda, K.; Katayama, M.; Kubota, J.; Yamada, A.; Konagai, M.; Domen, K. Photoelectrochemical Water Splitting Using a Cu(In,Ga)Se<sub>2</sub> Thin Film. *Electrochim. Commun.* **2010**, *12*, 851–853.
59. Tran, P. D.; Batabyal, S. K.; Pramanik, S. S.; Barber, J.; Wong, L. H.; Loo, S. C. J. A Cuprous Oxide-Reduced Graphene Oxide (Cu<sub>2</sub>O-rGO) Composite Photocatalyst for Hydrogen Generation: Employing rGO as an Electron Acceptor To Enhance the Photocatalytic Activity and Stability of Cu<sub>2</sub>O. *Nanoscale* **2012**, *4*, 3875–3878.
60. McKone, J. R.; Pieterick, A. P.; Gray, H. B.; Lewis, N. S. Hydrogen Evolution from Pt/Ru-Coated p-Type WSe<sub>2</sub> Photocathodes. *J. Am. Chem. Soc.* **2013**, *135*, 223.
61. Grimes, C. A.; Mor, G. K. *TiO<sub>2</sub> Nanotube Arrays: Synthesis, Properties, and Applications*; Springer: Berlin, 2009; pp 153–156.
62. Bard, A. J. Inner-Sphere Heterogeneous Electrode Reactions. *Electrocatalysis and Photocatalysis: The Challenge*. *J. Am. Chem. Soc.* **2010**, *132*, 7559–7567.
63. Wen, Z.; Cui, S.; Pu, H.; Mao, S.; Yu, K.; Feng, X.; Chen, J. Metal Nitride/Graphene Nanohybrids: General Synthesis and Multifunctional Titanium Nitride/Graphene Electrocatalyst. *Adv. Mater.* **2011**, *23*, 5445–5450.